Submitted to Energy & Environmental Science

Electronic Supplementary Information

Scalable Fabrication of MnO_2 Nanostructure Deposited on Free-standing Ni Nanocone Arrays for Ultrathin, Flexible, High-performance Micro-supercapacitor

Zijin Su, Cheng Yang, Binghe Xie, Ziyin Lin, Zhexu Zhang, Jingping Liu, Baohua Li, Hongda Du, Feiyu Kang, Ching Ping Wong

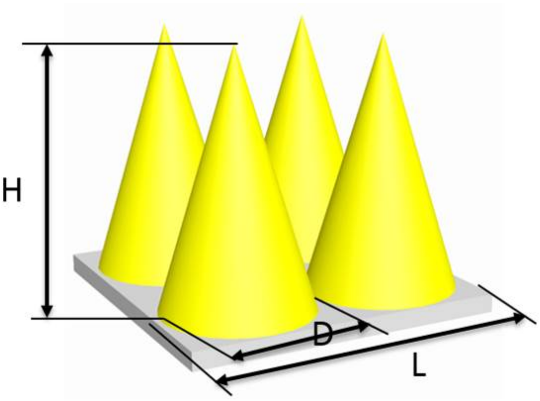

Scheme S1. Surface area calculation modeling. H-heigth of Ni nanocone (H=1200 nm), D-bottom diameter of Ni nanocone, L-length of the square substrate (L=2D). The average apex of the cone(θ) is about 30°.

The effective surface area (S) of Ni nanocones electrode in a L×L square substrage (including the side area of cones (S1) and the planar area excluding the undersite area of cones (S2)) can be calculated under the following equation:

$$S = S1 + S2 = 4 \times \pi\left(\frac{D}{2}\right)^2 \times \frac{1}{sin\left(\frac{\theta}{2}\right)} + 4 \times \{D^2 - \pi\left(\frac{D}{2}\right)^2\}$$

The surface area of the planar electrode (P) in the same substrate is :

$$P = L \times L = 4D^2$$

The ratio of the surface area between Ni naocone electrode and Ni planar electrode can be calculated by S/P, therefore, is 3.25.

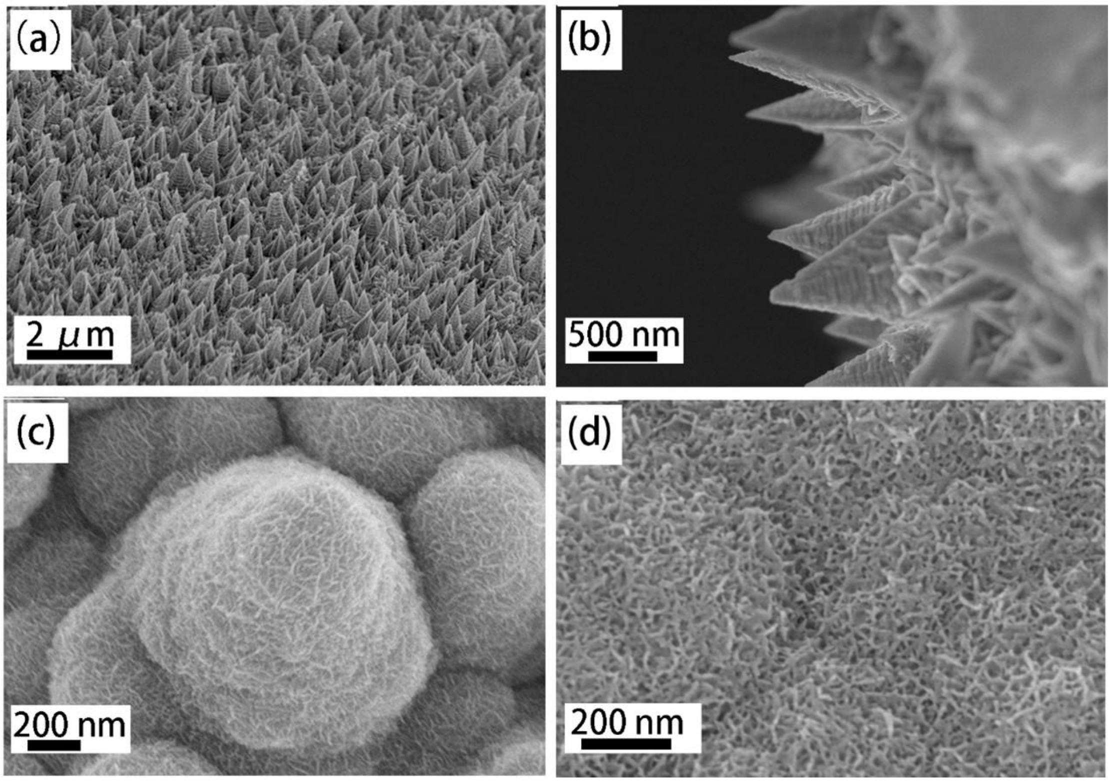

Fig. S1 (a) The low magnification SEM image of NCAs. (b) Side view of NCAs. (c)The magnified SEM image of MNN. (d) SEM images of the MnO_2 nanostructure deposited on a smooth Ni plate (control sample).

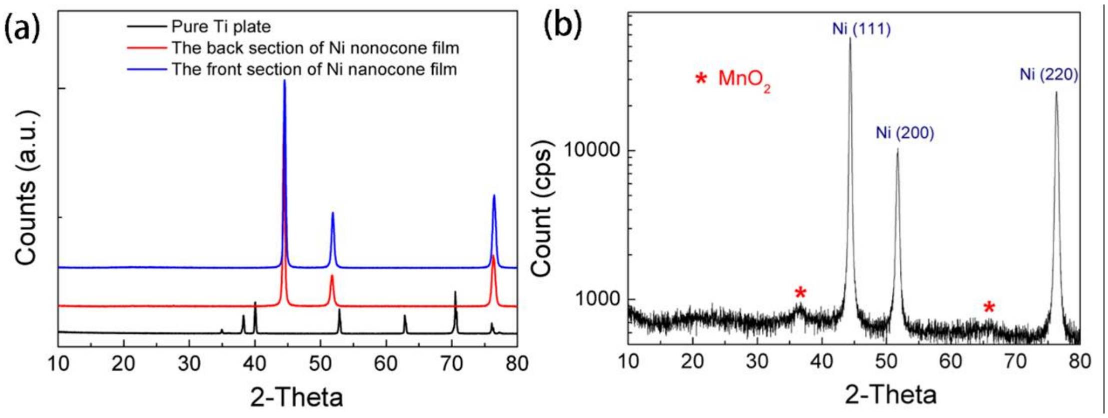

Fig. S2 (a) The phases of the front section and the back section of the film were tested by XRD. The result demonstrates that even the back section of thin film is Ni other than Ti. (b) XRD pattern of the MnO_2 nanostructure deposited on Ni naocones.

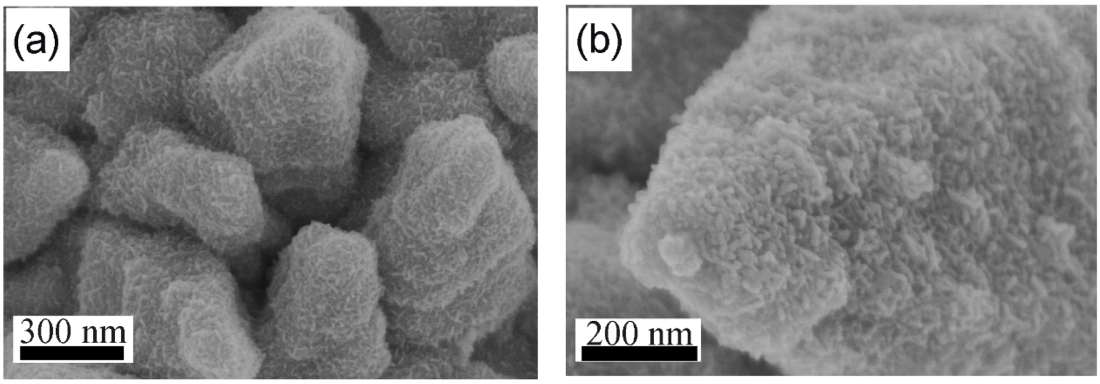

Fig. S3 SEM (a) and magnified SEM (b) images of MNN after 100 CV cycles with the scan rate of 20mV/s. There is not obvious morphology change of the MNN electrode after cyclic tests which demonstrates the high structure stability of the NCAs-based electrode.

Fig. S3a and b show that there is not noticeable change for the overall appearance of the MNN electrode after 100 CV cycles with the scan rate of 20mV/s. Though, the morphology of the deposited MnO_2 may have some small change with the scan rate and the number of CV cycles increase. The hierarchical structure of MnO_2/NCAs still keeps the same indicating the good structure integrity of MNN electrode.

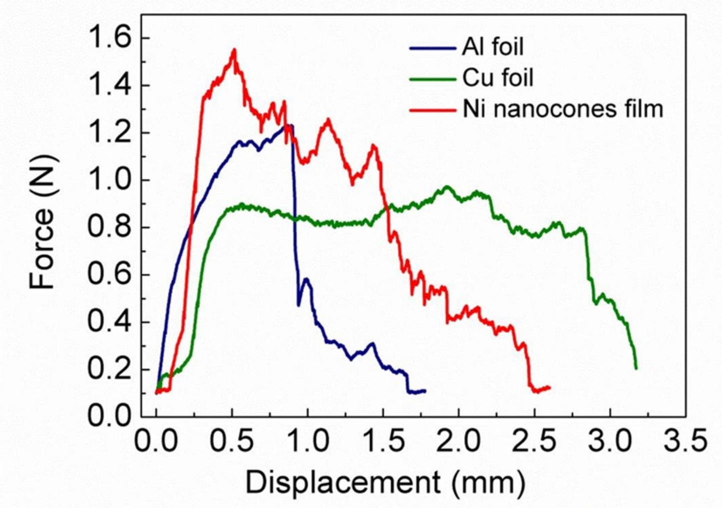

Fig. S4 The mechanical test of Ni nanocones film compared with that of Al and Cu foil.

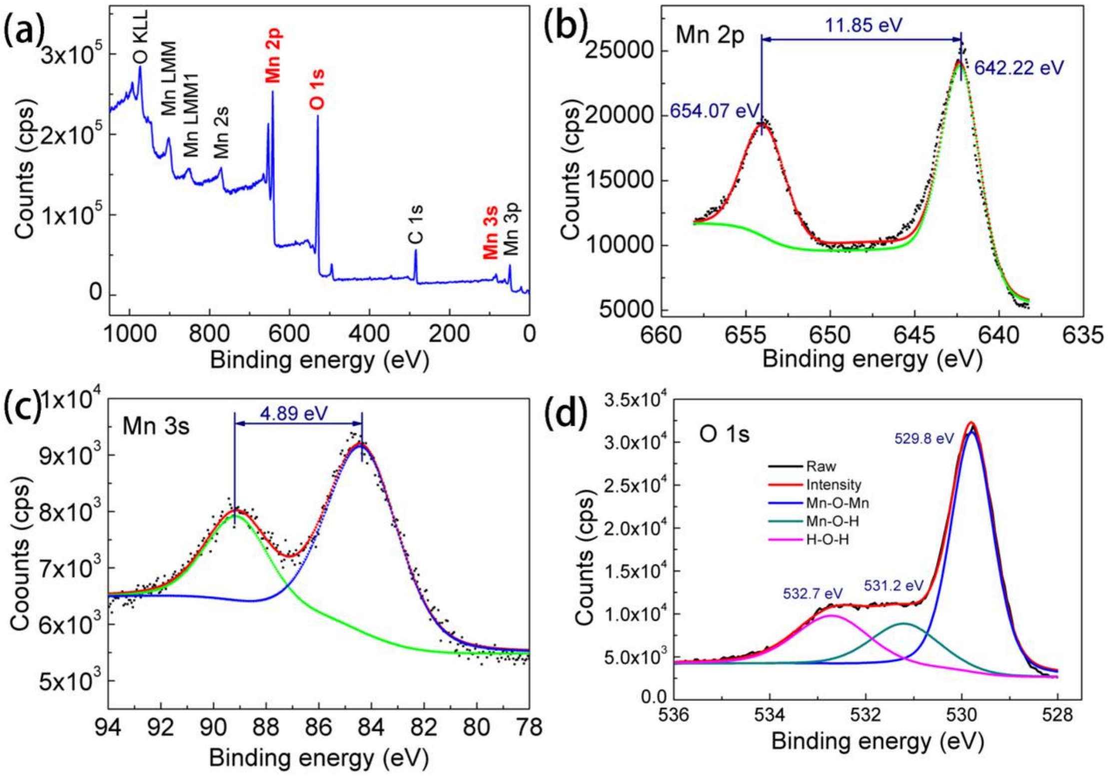

Fig. S5 (a) The XPS full spectrum of MnO_2 deposited on the NCAs. The full spectrum containing signals from Mn and O demonstrates the presence of MnO_2. The (b) Mn 2p, (c) Mn 3s, (d) O 1s core level XPS spectrum of MnO_2.

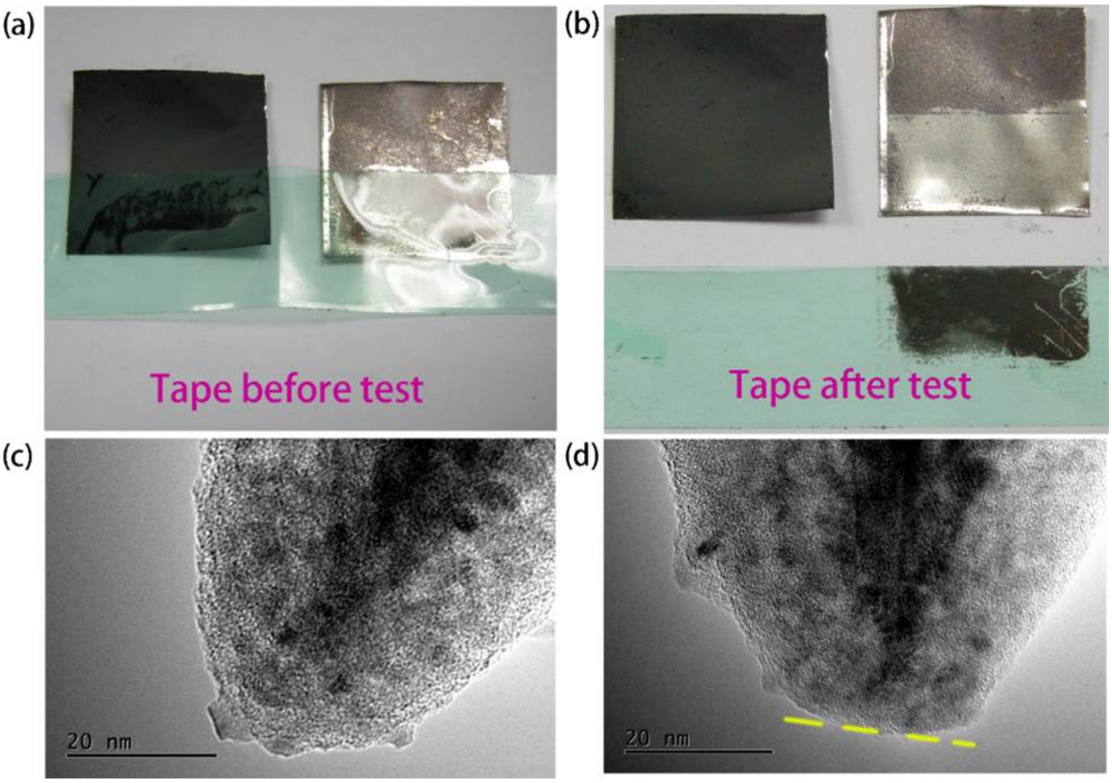

Fig. S6 The comparison adhesion test of MNN and MNP. (a) Tape was pasted to MNN and MNP.

(b) Tape was peeled off from MNN and MNP. There is no obvious change for MNN. However MNP shows a large amount of powder residues detached from the electrode. TEM images of MNN before (c) and after (d) adhesion test.

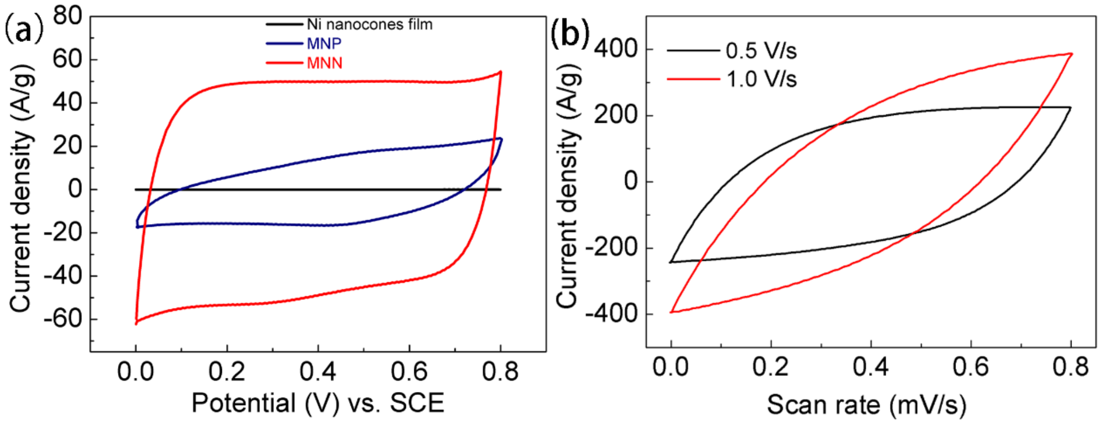

Fig. S7 (a) CV curves of Ni nanocones film, MNP, MNN at 100 mV/s in 0.5 M Na_2SO_4 electrolyte. The almost negligible CV area of Ni naoncones film indicates MnO_2 contribute to the most of the capacitance. The larger CV area of MNN compared with that of MNP demonstrates the higher specific capacitance as the result of nanostructure. (b) CV curves of MNN at scan rate of 0.5 V/s and 1.0 V/s. The similar rectangular of CVs indicates an excellent rate performance.

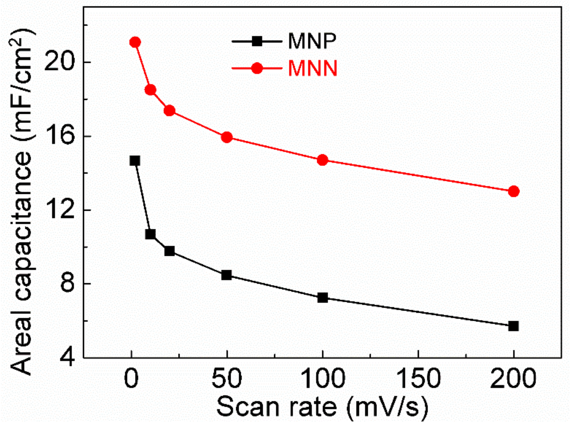

Fig. S8 The areal capacitance *vs.* scan rate curves with the same mass loading of 0.05 mg/cm^2 for MNN and MNP electrodes. The areal capacitance of MNN is consistently higher than that of MNP.

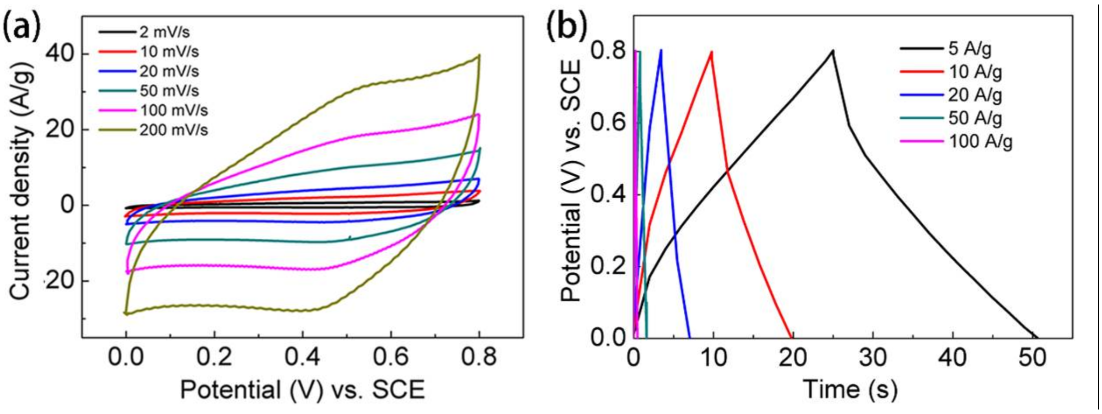

Fig. S9 (a) CV curves of MNP electrode at different scan rates. (b) GCD curves of MNP obtained at different current density from 5 to 100 A/g. The larger voltage drop of MNN indicates a higher internal resistance.

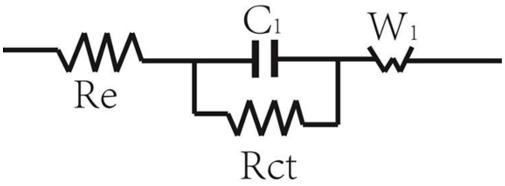

Fig. S10 The electrical equivalent circuit used for fitting impedance spectra.

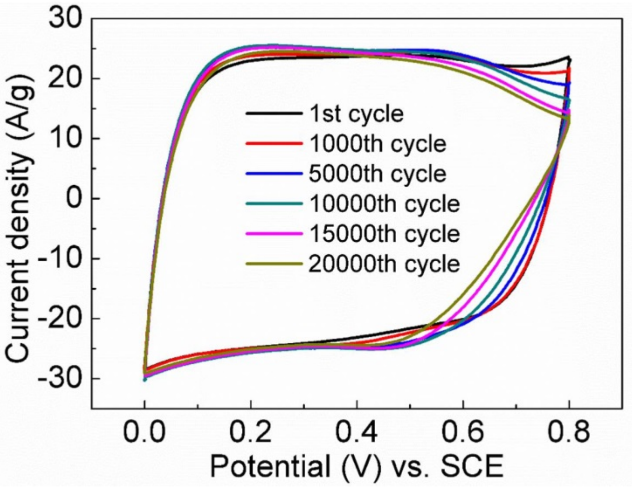

Fig. S11 CV curves of different cycles from the first to the 20, 000th cycle at 50mV/s. The CVs still remain rectangular even at the 20, 000th cycle.

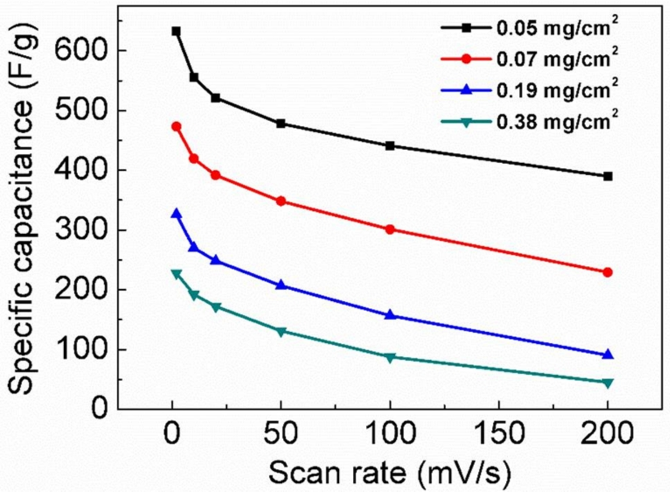

Fig. S12 The specific capacitance *vs.* scan rate curves with different mass loading of MnO_2.

The mass loading of MnO_2 can be increased by extending the deposition time. The specific decreases with the increase of scan rate and mass loading. Low scan rate is good for taking full advantage of the active materials. With the mass loading increases, the specific capacitance decreases due to the kinetics of the ion transport in the electrodes with low ion diffusion constants.

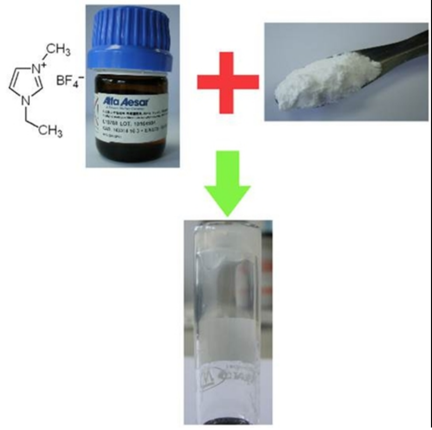

Fig. S13 The preparation of ionogel electrolyte based on ionic liquid and fumed silica (FS). The gel electrolyte was prepared by mixing together 1-Ethyl-3-methylim idazolium tetrafluoroborate ($EMIMBF_4$) with fumed silica nanopowder (1 ml $EMIMBF_4$/ 400mg FS). This mixture was stirred in glove box under an Ar atmosphere for more than 5 hours to get a clear viscous ionogel (FS-IL) for the asymmetric supercapacitor devices. The all-solid-state asymmetric supercapacitors using the ionogel electrolyte are capable of providing 2.5 V compare with 2.0 V for the Na_2SO_4 electrolyte. The increase of the voltage leads to the increase of energy density of the supercapacitors.

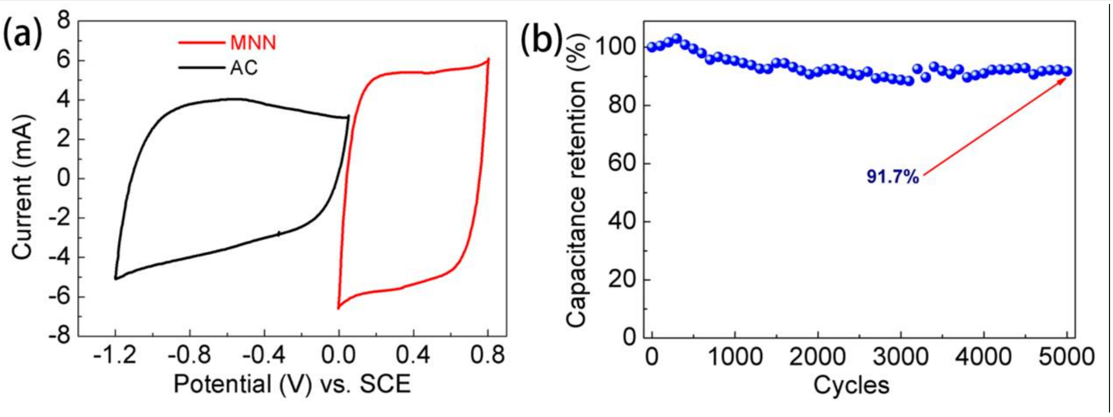

Fig. S14 (a) Comparative CV curves of MNN and AC electrodes performed in 0.5 M Na_2SO_4 aqueous solution at scan rate of 50 mV/s. (b) Capacitance retention of MNN/AC ionogel supercapaictor as a function of cycling number. The capacitance retention of the asymmetric supercapacitor remains as high as 91.7% after 5000 cycles.

Before the asymmetric supercapcitors fabrication, CV measurements were performed on MNN and AC electrode in 0.5 M Na_2SO_4 aqueous solution to estimate the stable potential windows. The potential window of MNN is 0-0.8 V. And the AC has a wide potential of -1.2- 0.05 V (Fig. S13a).

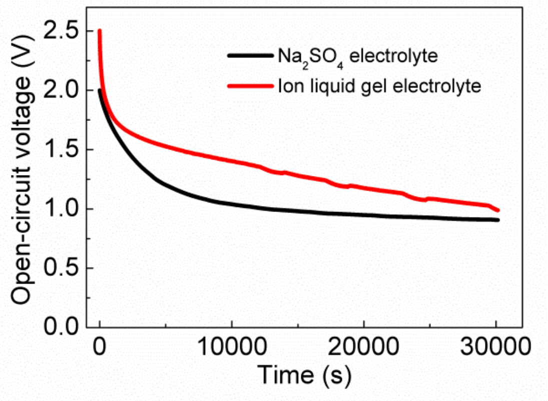

Fig. S15 Leakage current measurement of asymmetric supercapacitors based 0.5 M Na_2SO_4 electrolyte (black) and ionogel electrolyte (red). The supercapacitors were charged to 2.5 V and 2.0 V, respectively. The aqueous and ionogel supercapacitors took more than 8 h to drop to 0.9V and 1.0 V, respectively.

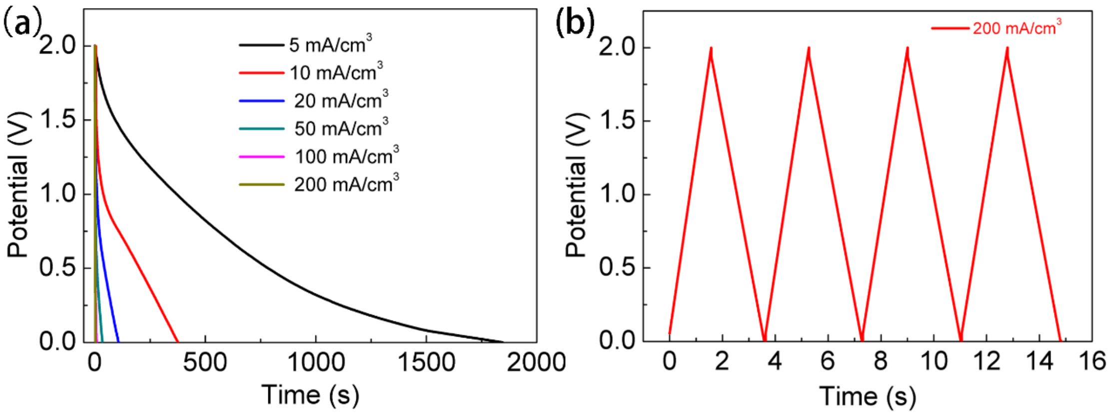

Fig. S16 (a) The discharge curves at different current densities and (b) the GCD curves at 200 mA/cm^3 of MNN/AC ionogel supercapaictors.

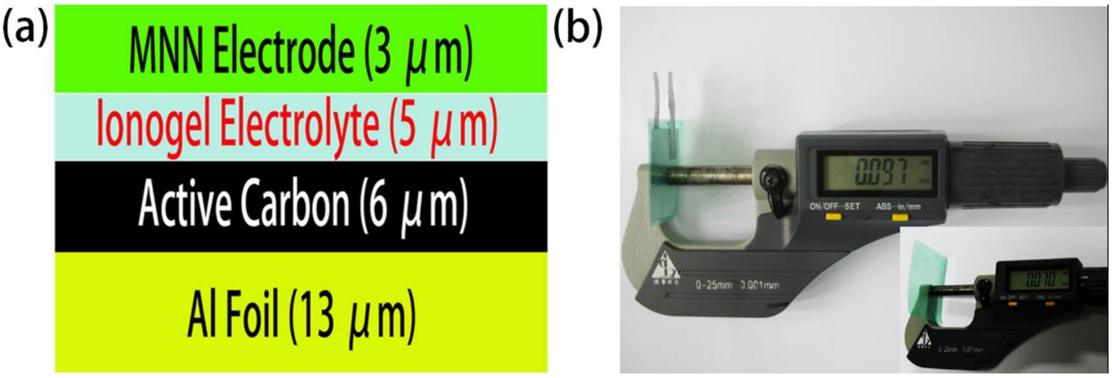

Fig. S17 (a) The sandwich structure of as-design supercapacitor. The total thickness of the ultrathin supercapacitor is as thin as 27 μm (exclude the PET package). (b) The thickness test of MNN/AC supercapacitor. The thickness of the full supercapacitor including the PET package (inset, 70 μm) is 97μm.

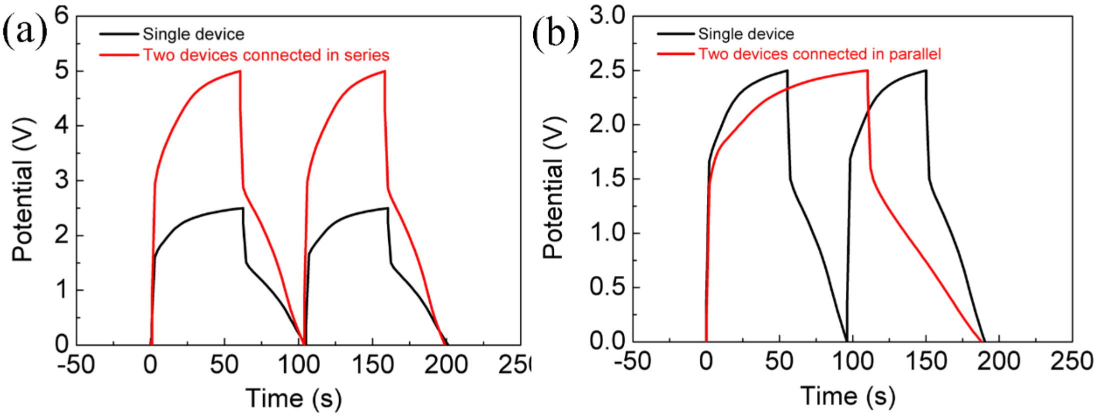

Fig. S18 GCD curves for two tandem microsupercapacitors connected (a) in series and (b) in parallel.

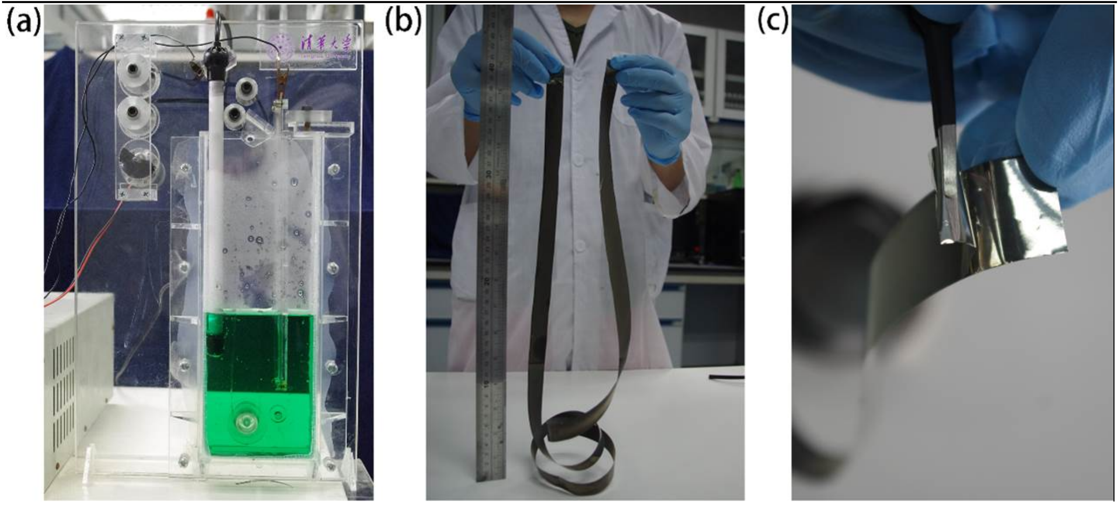

Fig. S19 (a) The as-design roll-to-roll device. The rolling speed is controlled by a motor integrated in the device. A heating rod is put in the ion solution to maintain a working temperature of 60 ℃. (b) As-prepare NCAs deposited on Ti plate by roll-to-roll process. The length of electrode is 1.3 m. (c) The demonstration of NCAs film peeled off from Ti substrate.